Kingdom of Saudi Arabia
Imam Muhammad Ibn Saud Islamic
University (IMSIU)
Faculty of Science
Department of Applied Physics

Investigation of radiation shielding properties of modified glass systems using Geant4 modelling software

A graduation project submitted to the Department of Applied Physics in partial fulfillment of the requirements
for the degree of Bachelor of Science in
Applied Mathematics

by

Hadeel AL-Qahtani

Kholoud AL-Anazi

Supervised by

Muneerah Alaqeel

June 14, 2025

Contents

List of Figures

List of Tables

Acknowledgements

"My mother's prayer, my father's silent pride — these are the winds beneath my wings."

We would like to express our sincere and heartfelt gratitude to our supervisor, Dr. Muneerah Al-Aqeel, whose kind guidance, valuable advice, and continuous encouragement played a key role in the success of this graduation project. Her belief in us gave us the confidence to keep pushing forward, even through moments of uncertainty.

To our families – you are the quiet force behind every accomplishment. To our mothers, whose prayers protected us in silence, and to our fathers, whose pride gave us strength. You have been our safe haven, our light, and our reason to keep striving. Thank you for every word of support, every gesture of love, and every sacrifice that helped us reach this point.

Finally, we humbly acknowledge that the completion of this work was only made possible by the grace and favor of Allah. All praise and thanks are due to Him, always and forever.

Hadeel Al-Qahtani & Kholoud AL-Anazi

Abstract

The development of effective radiation shielding materials remains a critical priority across medical, nuclear, and industrial sectors. Among alternative materials, modified glass systems have gained attention due to their compositional flexibility, optical transparency, and potential for attenuation of both gamma rays and neutrons. This study investigates the shielding capabilities of five glass samples with varying compositions using Monte Carlo-based `Geant4` and the analytical `EpiXS` tool.

Key shielding parameters—including the mass attenuation coefficient (μ/ρ), half-value layer (HVL), and macroscopic removal cross-section (ΣR)—were calculated across a broad energy range (0.01–20 MeV). The results demonstrated strong agreement between the simulation outputs from Geant4 and the theoretical values from EpiXS, confirming the validity of the computational approach. Sample 3 exhibited the highest performance in terms of neutron attenuation, while Sample 2 provided consistent shielding across energy ranges.

The study highlights the significant influence of dopants such as Bi_2O_3, PbO, and WO_3 on enhancing attenuation properties. These findings support the use of doped glass systems as viable, lead-free alternatives for radiation shielding in high-exposure environments.

Chapter 1

Introduction

1.1 Background

Radiation protection has become a critical concern in numerous applications, including nuclear power generation, medical diagnostics, radiotherapy, and industrial radiography. Prolonged exposure to ionizing radiation can lead to severe biological consequences, such as DNA damage, genetic mutations, and cancer. Accordingly, the development of effective shielding materials is essential to minimize radiation exposure and ensure both occupational and environmental safety.

Traditionally, materials such as lead and other dense metals have been employed for radiation shielding due to their high atomic numbers and superior attenuation capabilities. However, these materials suffer from several disadvantages, including toxicity, heaviness, environmental hazards, and difficulty in manufacturing, handling, and disposal. These limitations have encouraged the search for alternative shielding materials that are safer, lighter, and more versatile.

Among these alternatives, glass-based materials have emerged as promising candidates for radiation protection. Glass offers unique advantages such as ease of fabrication, optical transparency, excellent chemical and thermal stability, and the ability to be doped with various elements to tailor its properties [1]. One key strategy for enhancing the radiation attenuation capacity of glass is doping with high atomic number oxides such as Bi_2O_3, PbO, and WO_3. These heavy metal oxides (HMOs) significantly increase the material's density and interaction cross-sections, thereby improving gamma and neutron absorption [1]. Additionally, doping alters the mechanical strength and optical clarity of the glass, making the balance between attenuation efficiency and physical integrity a central challenge in material development.

1.2 Motivation

While considerable progress has been made in the development of radiation-shielding glasses, much of the existing research has focused on attenuation of gamma rays, with relatively limited

data available regarding neutron shielding performance. Moreover, many studies differ in their experimental and computational methods, making direct comparisons between glass systems difficult. This gap in consistent and comprehensive evaluation has created a need for standardized investigations that assess both gamma and neutron shielding in unified simulations.

This study aims to address these gaps by evaluating the shielding properties of multiple glass samples doped with heavy metal oxides using `Geant4` and `EpiXS` simulation tools. The objective is to determine which compositions optimize the trade-off between attenuation performance, mechanical stability, and optical transparency. Ultimately, these optimized materials could serve as viable, environmentally safer alternatives to conventional shielding substances for use in medical, industrial, and nuclear settings [2].

1.3 Recent Advances in Radiation Shielding Glass

In recent years, the development of radiation shielding glass systems has garnered significant attention, particularly with the adoption of Monte Carlo simulation techniques such as `Geant4` [3]. Several studies have demonstrated that appropriate doping of glass matrices with high-Z oxides can significantly enhance their ability to attenuate both gamma and neutron radiation.

Sayyed [1] investigated Bi_2O_3–B_2O_3–SiO_2–Na_2O glasses using Geant4 and showed that the addition of Bi_2O_3 greatly improved photon attenuation efficiency across a wide energy spectrum. Similarly, Isazadeh and Saray [4] evaluated the shielding performance of CaF_2–CaO–B_2O_3–P_2O_5–SrO–Ta_2O_5 glass systems using both Geant4 and MCNPX codes, highlighting the positive impact of Ta_2O_5 in enhancing high-energy radiation shielding. In another study, Zaid et al. [5] demonstrated that BaO-doped borate glasses exhibited improved attenuation at lower energy levels, while Hendi et al. [6] explored TeO_2–V_2O_5–Bi_2O_3 systems, which showed strong gamma attenuation due to the presence of multiple high-Z elements.

More recently, Eisawy et al. [7] conducted a comprehensive study assessing neutron and gamma shielding capabilities of various glass compositions enriched with Bi_2O_3, Sb_2O_3, and Ta_2O_5 using NXCOM simulations. Their findings demonstrated the superior performance of their Sy3 sample, which recorded the highest macroscopic removal cross-section (ΣR) and the lowest Half-Value Layer (HVL) values among the tested compositions. This study reinforces the importance of selecting specific dopants and optimizing their concentrations to achieve reliable and efficient shielding behavior in glass matrices.

Collectively, these contributions underscore the growing relevance of simulation-based evaluation in radiation shielding research and highlight the effectiveness of high-Z dopants such as Bi_2O_3, Ta_2O_5, and Sb_2O_3. Building on this foundation, the present study employs both `Geant4` and `EpiXS` tools to assess the gamma and neutron attenuation properties of newly designed glass samples across a broad energy range, with the aim of identifying formulations that combine radiation resistance, mechanical robustness, and optical clarity [2, 8, 9].

Chapter 2

Theory Concepts

2.1 Interaction of Radiation with Matter

Radiation interactions with modified glass systems are governed by both the properties of the incoming radiation and the atomic structure of the glass. This chapter provides an overview of the major interaction mechanisms for gamma rays and neutrons, in addition to the key physical concepts used to assess radiation shielding performance in glass-based materials [8, 9].

2.1.1 Gamma Radiation Interactions

Gamma rays interact with matter through three primary mechanisms: photoelectric absorption, Compton scattering, and pair production. The significance of each interaction depends on the photon energy and the atomic number of the material [8].

2.1.1.1 Photoelectric Absorption

A gamma photon is completely absorbed by an inner-shell electron, ejecting it from the atom. This process dominates at low photon energies and in materials with high atomic numbers [8, 9]. The energy relationship is expressed by:

$$E_\gamma = E_B + E_k$$

2.1.1.2 Compton Scattering

A gamma photon scatters off a loosely bound or free electron, transferring part of its energy to the electron [8, 9]. The energy of the scattered photon is given by:

$$E' = \frac{E_\gamma}{1 + \frac{E_\gamma}{m_e c^2}(1 - \cos\theta)}$$

where E' is the energy of the scattered photon, E_γ is the initial photon energy, m_e is the electron mass, c is the speed of light, and θ is the scattering angle. The differential cross-section is given by the Klein-Nishina formula [8, 9]:

$$\frac{d\sigma}{d\Omega} = \frac{r_0^2}{2}\left(\frac{1+\cos^2\theta}{[1+\alpha(1-\cos\theta)]^2}\right)\left[1+\frac{\alpha^2(1-\cos\theta)^2}{(1+\cos^2\theta)[1+\alpha(1-\cos\theta)]}\right]$$

where $\alpha = \frac{h\nu}{m_e c^2}$ is the dimensionless photon energy, r_0 is the classical electron radius, and θ is the scattering angle (Figure 2.1).

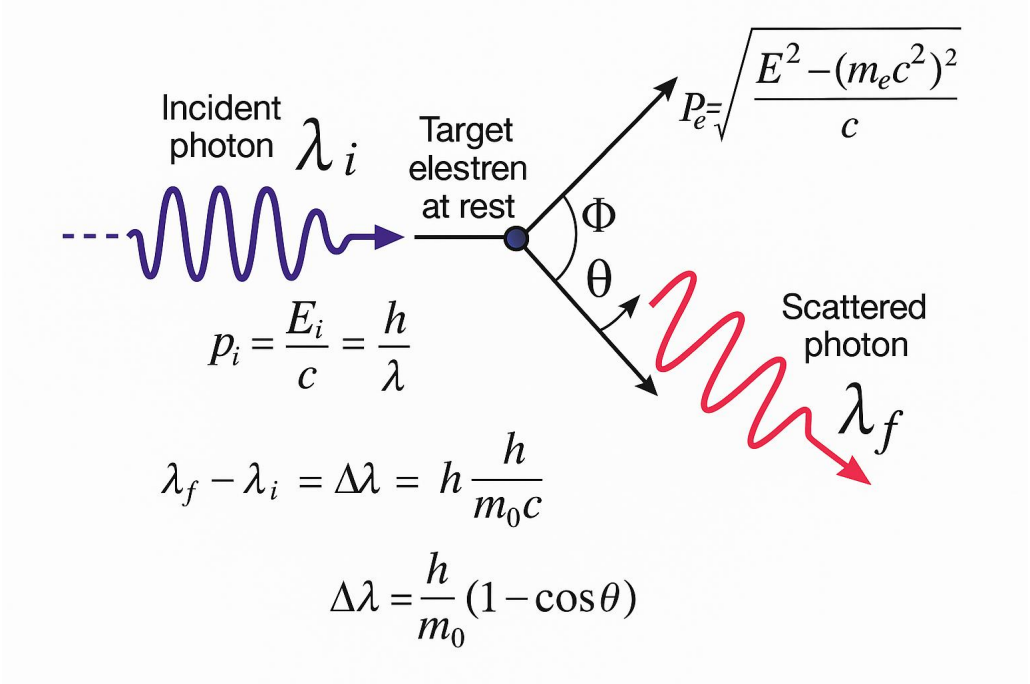

Figure 2.1: Compton Scattering.

2.1.1.3 Pair Production

Pair production occurs when a high-energy gamma photon, with energy exceeding 1.022 MeV, interacts with the electromagnetic field of a nucleus, resulting in the creation of an electron-positron pair [8, 9]. This process is particularly significant in materials enriched with heavy metal oxides such as Bi_2O_3, PbO, and Sb_2O_3, which are commonly used in modified glass systems to enhance gamma-ray attenuation [1].

The threshold energy for pair production is defined by:

$$E_{\text{threshold}} = 2m_e c^2 = 1.022 \text{ MeV} \tag{2.1}$$

where $E_{\text{threshold}}$ is the minimum energy required for the process, m_e is the electron mass, and c is the speed of light. This mechanism dominates at high photon energies, complementing photoelectric absorption at low energies and Compton scattering at intermediate energies [8].

2.2 Neutron Interactions with Matter

Neutrons, along with protons, form the core components of atomic nuclei. Due to their neutral electric charge, neutrons interact with matter exclusively through nuclear forces, unlike charged particles that are influenced by Coulomb barriers. This absence of electric charge allows neutrons to penetrate atomic nuclei more easily, resulting in a higher probability of nuclear interactions. This probability is represented by the cross-section, a key parameter in evaluating neutron interactions with materials [9].

This section examines the fundamental characteristics of neutron interactions, with a particular focus on cross-section measurements and the methods used to calculate interaction rates.Understanding these parameters is crucial for optimizing radiation shielding materials and enhancing neutron attenuation efficiency in modified glass systems [8, 9].

2.2.1 Types of Neutron Interactions

Neutron interactions with nuclei are generally classified into two main categories: **scattering** and **absorption** [8].

2.2.2 Scattering

In scattering interactions, a neutron collides with a nucleus, and both particles remain intact after the reaction. These interactions are commonly represented as (n, n) and are divided into two types [9]:

2.2.2.1 Elastic Scattering

In this process, the total kinetic energy of the neutron and the nucleus is conserved. The energy is merely redistributed between the two particles without causing any excitation of the nucleus. This type of scattering is effective for neutron moderation, especially in materials with low atomic mass such as **boron-based glass (B_2O_3-doped glass)** and **SiO_2 composites** used in radiation shielding [8].

2.2.2.2 Inelastic Scattering

In this process, a portion of the neutron's kinetic energy is transferred to the nucleus, causing it to become excited. The excited nucleus then releases this excess energy by emitting gamma rays. Heavy metal oxides like **Bi_2O_3, PbO, and Sb_2O_3** are particularly effective in modified glass systems, enhancing neutron attenuation through inelastic scattering mechanisms [1].

2.2.3 Scattering in Neutron Moderation

Scattering reactions are critical for moderating neutrons in shielding applications. Neutrons typically possess energies around 2 MeV, and must be slowed to thermal energies (eV range). This moderation process occurs via successive scattering events within the glass matrix, utilizing materials such as $\mathbf{B_2O_3}$ and $\mathbf{SiO_2}$ as neutron moderators [8, 9].

2.2.4 Absorption

In absorption interactions, a neutron is captured by a nucleus, resulting in nuclear reactions such as neutron capture with gamma emission, alpha particle emission, or nuclear fission. Examples of these absorptive reactions are shown in Table 2.1 [8, 9].

Reaction	Name
$n + {}^{A}_{Z}X \rightarrow {}^{A-1}_{Z+1}Y + p$	(n, p) reaction
$n + {}^{A}_{Z}X \rightarrow {}^{A-4}_{Z-2}Y + \alpha$	(n, α) reaction
$n + {}^{A}_{Z}X \rightarrow {}^{A-1}_{Z}X + 2n$	$(n, 2n)$ reaction
$n + {}^{A}_{Z}X \rightarrow {}^{A}_{Z}X + \gamma$	(n, γ) reaction
$n + {}^{A}_{Z}X \rightarrow {}^{A}_{Z_1}Y_1 + {}^{A_2}_{Z_2}Y_2 + n + n + \ldots$	fission

Table 2.1: Examples of Absorptive Neutron Reactions

2.2.5 Radiation Attenuation

Modified glass systems offer significant advantages as radiation shielding materials due to their transparency, structural stability, and capability for incorporating high-Z elements such as heavy metal oxides [1].

The gamma ray attenuation behavior can be described by Beer–Lambert's law [8, 9]:

$$I = I_0 e^{-\mu x}$$

Where μ represents linear attenuation coefficient, and μ_m, HVL, and MFP parameters define shielding effectiveness [8, 9].

$$\text{HVL} = \frac{\ln 2}{\mu}, \quad \text{MFP} = \frac{1}{\mu}$$

Neutron shielding effectiveness is quantified by effective removal cross-section Σ_R [9].

This study leverages Geant4 to evaluate shielding performance, contributing valuable insights into advanced shielding designs [3].

Chapter 3

Methodology

3.1 Simulation Design

The simulation was developed using a hybrid approach combining Monte Carlo methods via `Geant4` and analytical calculations using tools such as `EpiXS` and `NXCom` [2, 3]. The NXCom code has been validated in previous studies for accurately estimating macroscopic removal cross-sections in complex glass systems [7], supporting its selection as a reliable tool for neutron interaction analysis.

Five distinct glass samples—whose chemical compositions and physical properties are summarized in **Table 3.1** were assigned realistic physical parameters, including density and elemental makeup. `Geant4` was employed to simulate gamma and neutron interactions within these samples, focusing on radiation transport, absorption, and scattering behavior within the materials.

3.2 Radiation Sources

Two types of radiation sources were utilized in this study:

1. **Gamma rays**: The gamma radiation sources were modeled with energies ranging from 10 keV to 20 MeV, covering a comprehensive spectrum of energy levels commonly encountered in various applications.
2. **Neutrons**: Neutron sources were configured with energies ranging from 10 keV to 20 MeV, allowing for the evaluation of neutron shielding capabilities across different energy ranges.

The sources were positioned at a fixed distance of 20 cm from the glass sample to ensure uniform irradiation [8, 9].

3.3 Physics Models

Geant4 offers a variety of physics models to simulate particle interactions. For this study, the following models were employed [3]:

- **Electromagnetic interactions**: The Livermore and Penelope models were used for gamma ray interactions to simulate photoelectric effect, Compton scattering, and pair production [8, 9].
- **Hadronic interactions**: The High Precision (HP) neutron model was applied to simulate neutron scattering, absorption, and other nuclear processes relevant to neutron attenuation.

3.4 Detector Configuration

To measure the attenuation properties of the **glass material**, virtual detectors were placed:

- **Before the sample**: To measure the initial intensity of radiation.
- **After the sample**: To measure the transmitted radiation intensity.

For each energy level, attenuation parameters such as the linear attenuation coefficient and neutron effective removal cross-sections were calculated [8, 9].

3.5 Data Analysis

The simulation data were analyzed to determine the material's radiation shielding effectiveness, focusing on key parameters such as the linear attenuation coefficient (LAC), which quantifies the glass material's ability to attenuate gamma rays; the neutron effective removal cross-sections, representing the material's capacity to reduce neutron energy and flux; the mean free path (MFP), which indicates the average distance a particle travels in the glass before an interaction occurs; and the half-value layer (HVL), which denotes the thickness required to reduce radiation intensity by half [8, 9].

Data for gamma rays were compared with results obtained from EpiXS simulations to evaluate the consistency and accuracy of Geant4. Neutron shielding properties were exclusively evaluated using Geant4 due to the unique nature of the neutron interactions with the glass samples [3].

3.6 Summary

This methodology combines Monte Carlo simulation (Geant4) with analytical tools (EpiXS and NXCom) to thoroughly assess gamma and neutron shielding properties of glass materials with varied compositions. Incorporating heavy metal oxides within glass matrices optimizes radiation protection while maintaining optical transparency, making these materials promising candidates for practical radiation shielding applications [1].

Table 3.1: Chemical compositions and physical properties of the five glass samples.

System1: $45B_2O_3$+$20Bi_2O_3$+$20Na_2O_2$+$15Sb_2O_3$							
Weight fraction (mol%)		Elemental composition		Density (g/cm³)	(n)	Molar weight	Weight fraction
B_2O_3	45%	B	0.053			3132.9	17.04%
Bi_2O_3	20%	O	0.243			9319.2	50.69%
Na_2O_2	20%	Na	0.05	6.29	2.5635	1559.6	8.48%
Sb_2O_3	15%	Bi	0.455			4372.8	23.78%
		Sb	0.199			Total = 18384.5 g/mol	
System2: $20Bi_2O_3$-$60B_2O_3$-10PbO-$10TiO_2$							
Weight fraction (wt%)		Elemental composition		Density (g/cm³)	(n)	Molar weight	Weight fraction
B_2O_3	60%	B	0.186343			4177.2	25.27%
Bi_2O_3	20%	O	0.483653			9319.2	56.39%
PbO	10%	Ti	0.059941	5.05	2.421	2232	13.51%
TiO_2	10%	Pb	0.090665			798.7	4.83%
		Bi	0.179398			Total = 16527.1 g/mol	
System3: $50Bi_2O_3$-$12.5WO_3$-37.5PbO							
Weight fraction (mol%)		Elemental composition		Density (g/cm³)	(n)	Molar weight	Weight fraction
Bi_2O_3	50%	W	0.1145			23298	67.40%
WO_3	12.5%	Pb	0.1124	10.664	2.6	2898	8.38%
PbO	37.5%	Bi	0.2146			8370	24.21%
		O	0.5585			Total = 34566 g/mol	
System4: $30La_2O_3$-$70B_2O_3$							
Weight fraction (mol%)		Elemental composition		Density (g/cm³)	(n)	Molar weight	Weight fraction
La_2O_3	30%	O	0.32768			9774.6	66.73%
B_2O_3	70%	La	0.56898	3.7703	1.6537	4873.4	33.27%
		B	0.10333			Total = 14648 g/mol	
System5: $80TeO_2$-$10Bi_2O_3$-4ZnO-$6Ta_2O_5$							
Weight fraction (mol%)		Elemental composition		Density (g/cm³)	(n)	Molar weight	Weight fraction
TeO_2	80%	O	0.174488			12768	62.57%
Bi_2O_3	10%	Zn	0.046649			4659.6	22.84%
ZnO	4%	Te	0.455199	6.465	2.6153	325.52	1.60%
Ta_2O_5	6%	Ta	0.110659			2651.4	12.99%
		Bi	0.213005			Total = 20404.52 g/mol	

Chapter 4

Results and Discussion

4.1 Gamma Attenuation Coefficients

This section presents an analysis of five glass samples with different chemical compositions and densities to assess their effectiveness in attenuating gamma radiation. The **mass and linear attenuation coefficients** were determined using both **Geant4 Monte Carlo simulations** and theoretical calculations from the **EpiXS** program.

The percentage deviation between the results obtained from EpiXS and Geant4 was calculated using the following equation:

$$\text{Deviation}(\%) = \frac{\mu_l(\text{EpiXS}) - \mu_l(\text{Geant4})}{\mu_l(\text{EpiXS})} \times 100 \tag{4.1}$$

Where:

- μ_l(EpiXS) represents the linear attenuation coefficient obtained from EpiXS.
- μ_l(Geant4) represents the corresponding value from Geant4 simulations.

The mass attenuation coefficients (μ_m) for all samples were plotted over an energy range of **0.01 to 20 MeV**, as shown inFigures 4.1 to 4.5.

4.1.1 Half-Value Layers (HVL)

The **Half-Value Layer (HVL)** was calculated to evaluate the shielding efficiency of each glass sample. HVL indicates the material thickness required to reduce the gamma radiation intensity by 50%, making it a key factor in designing safe shielding environments.

Results from Geant4 and EpiXS were compared, and the deviation between both methods was calculated using Equation (4.1). Detailed HVL values are presented in Tables4.1 to 4.5

4.1.2 Results by Sample

4.1.2.1 Sample 1

The results for this sample are presented in Fig. 4.1 and Table 4.1.

4.1.2.2 Sample 2

The results for this sample are presented in Fig. 4.2 and Table 4.2.

4.1.2.3 Sample 3

The results for this sample are presented in Fig. 4.3 and Table 4.3.

4.1.2.4 Sample 4

The results for this sample are presented in Fig. 4.4 and Table 4.4.

4.1.2.5 Sample 5

The results for this sample are presented in Fig. 4.5 and Table 4.5.

Table 4.1: Linear Attenuation Coefficients and HVLs of Sample 1 obtained from EpiXS and Simulated by G4.

Energy (MeV)	EpiXS		G4		Error %	
	LAC (cm^{-1})	HVL (cm)	LAC (cm^{-1})	HVL (cm)	LAC	HVL
0.010	593.311	0.001	593.218	0.001	0.016	0.016
0.020	290.434	0.002	290.284	0.002	0.052	0.052
0.030	102.030	0.007	102.306	0.007	0.270	0.269
0.040	69.835	0.010	69.804	0.010	0.045	0.045
0.050	39.032	0.018	39.149	0.018	0.300	0.299
0.060	24.785	0.028	24.918	0.028	0.535	0.533
0.081	11.206	0.062	11.301	0.061	0.846	0.839
0.112	17.877	0.039	14.480	0.048	19.004	23.464
0.122	11.777	0.059	11.748	0.059	0.245	0.246
0.136	8.975	0.077	9.020	0.077	0.496	0.494
0.161	6.085	0.114	6.029	0.115	0.922	0.930
0.223	2.920	0.237	2.912	0.238	0.262	0.263
0.276	1.910	0.363	1.907	0.364	0.183	0.183
0.302	1.619	0.428	1.622	0.427	0.223	0.223
0.356	1.238	0.560	1.236	0.561	0.213	0.214
0.384	1.105	0.627	1.103	0.629	0.253	0.253
0.511	0.762	0.909	0.764	0.907	0.194	0.193
0.662	0.583	1.190	0.586	1.182	0.642	0.638
0.835	0.476	1.456	0.481	1.441	0.996	0.986
0.840	0.476	1.456	0.479	1.448	0.517	0.514
1.170	0.370	1.874	0.373	1.860	0.761	0.755
1.275	0.351	1.977	0.353	1.966	0.569	0.566
1.333	0.341	2.033	0.343	2.019	0.695	0.690
2.000	0.279	2.481	0.280	2.475	0.278	0.277
3.000	0.245	2.825	0.245	2.829	0.126	0.126
5.000	0.228	3.041	0.229	3.028	0.431	0.429
6.000	0.227	3.049	0.229	3.027	0.723	0.718
8.000	0.232	2.992	0.234	2.963	1.004	0.994
10.000	0.239	2.900	0.241	2.872	0.958	0.949
20.000	0.279	2.486	0.278	2.495	0.359	0.361

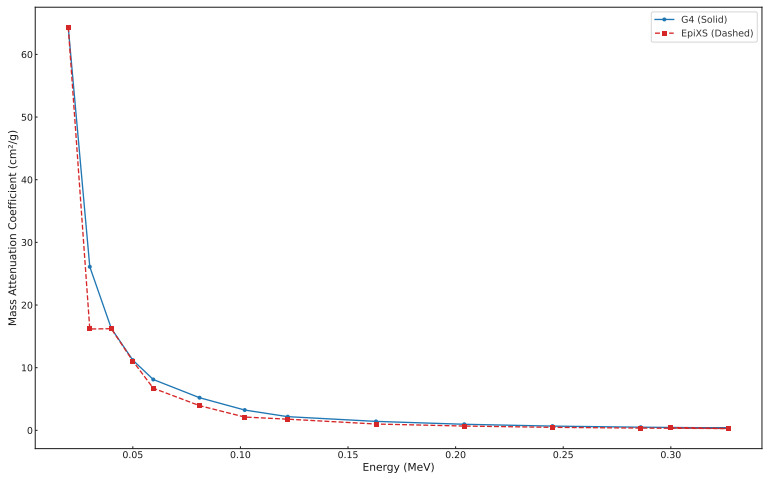

Figure 4.1: Comparison for Sample 1 between EpiXS data and simulated G4 data.

Table 4.2: Linear Attenuation Coefficients and HVLs of Sample 2 obtained from EpiXS and Simulated by G4.

Energy (MeV)	EpiXS		G4		Error %	
	LAC (cm^{-1})	HVL (cm)	LAC (cm^{-1})	HVL (cm)	LAC	HVL
0.010	452.303	0.002	452.331	0.002	0.006	0.006
0.020	286.037	0.002	285.802	0.002	0.082	0.082
0.030	101.111	0.007	101.107	0.007	0.003	0.003
0.040	48.007	0.014	48.003	0.014	0.009	0.009
0.050	26.931	0.026	26.946	0.026	0.054	0.054
0.060	17.186	0.040	17.293	0.040	0.624	0.620
0.081	7.872	0.088	7.989	0.087	1.495	1.473
0.112	17.152	0.040	13.905	0.050	18.931	23.352
0.122	11.303	0.061	11.277	0.061	0.228	0.229
0.136	8.606	0.081	8.647	0.080	0.479	0.477
0.161	5.816	0.119	5.758	0.120	0.990	1.000
0.223	2.749	0.252	2.741	0.253	0.308	0.309
0.276	1.770	0.392	1.766	0.393	0.230	0.230
0.302	1.488	0.466	1.491	0.465	0.227	0.227
0.356	1.120	0.619	1.118	0.620	0.241	0.242
0.384	0.992	0.698	0.989	0.701	0.309	0.310
0.511	0.665	1.042	0.666	1.041	0.104	0.104
0.662	0.497	1.395	0.500	1.387	0.544	0.542
0.835	0.400	1.735	0.403	1.719	0.924	0.916
0.840	0.400	1.735	0.401	1.728	0.410	0.408
1.170	0.305	2.271	0.308	2.254	0.750	0.744
1.275	0.289	2.402	0.290	2.389	0.546	0.543
1.333	0.280	2.473	0.282	2.456	0.660	0.656
2.000	0.229	3.029	0.229	3.024	0.162	0.162
3.000	0.201	3.443	0.201	3.450	0.206	0.207
5.000	0.188	3.690	0.189	3.670	0.569	0.566
6.000	0.188	3.694	0.189	3.660	0.928	0.919
8.000	0.192	3.616	0.194	3.570	1.301	1.285
10.000	0.198	3.498	0.201	3.454	1.290	1.274
20.000	0.232	2.983	0.232	2.988	0.172	0.172

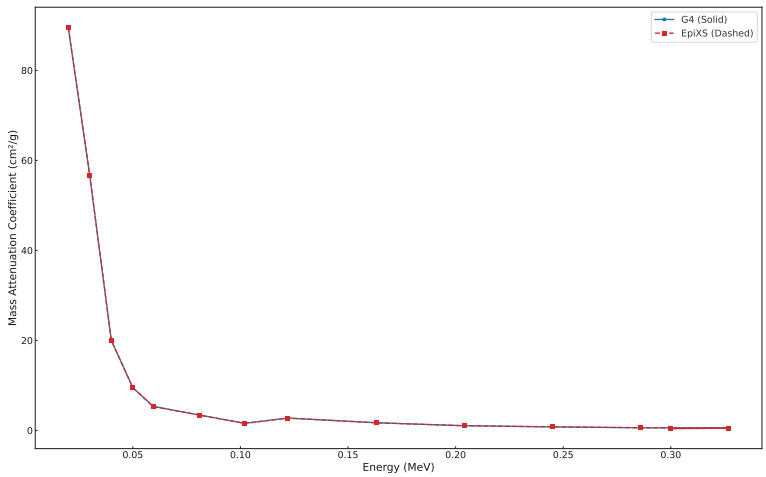

Figure 4.2: Comparison for Sample 2 between EpiXS data and simulated G4 data.

Table 4.3: Linear Attenuation Coefficients and HVLs of Sample 3 obtained from EpiXS and Simulated by G4.

Energy (MeV)	EpiXS		G4		Error %	
	LAC (cm^{-1})	HVL (cm)	LAC (cm^{-1})	HVL (cm)	LAC	HVL
0.010	1257.382	0.001	1355.230	0.001	7.782	7.220
0.020	829.282	0.001	826.086	0.001	0.385	0.387
0.030	292.674	0.002	291.754	0.002	0.314	0.315
0.040	138.601	0.005	138.176	0.005	0.307	0.308
0.050	77.463	0.009	77.283	0.009	0.232	0.232
0.060	49.198	0.014	49.376	0.014	0.363	0.361
0.081	26.399	0.026	26.479	0.026	0.303	0.302
0.112	49.757	0.014	40.109	0.017	19.389	24.053
0.122	32.583	0.021	32.419	0.021	0.501	0.504
0.136	24.677	0.028	24.731	0.028	0.217	0.216
0.161	16.510	0.042	16.300	0.043	1.273	1.289
0.223	7.570	0.092	7.527	0.092	0.565	0.569
0.276	4.735	0.146	4.712	0.147	0.487	0.489
0.302	3.923	0.177	3.923	0.177	0.016	0.016
0.356	2.873	0.241	2.859	0.242	0.509	0.511
0.384	2.511	0.276	2.496	0.278	0.595	0.599
0.511	1.597	0.434	1.594	0.435	0.188	0.188
0.662	1.142	0.607	1.146	0.605	0.326	0.325
0.835	0.889	0.780	0.896	0.774	0.772	0.766
0.840	0.889	0.780	0.891	0.778	0.186	0.185
1.170	0.656	1.057	0.661	1.049	0.763	0.758
1.275	0.617	1.124	0.620	1.118	0.539	0.536
1.333	0.598	1.159	0.602	1.151	0.636	0.632
2.000	0.490	1.414	0.491	1.413	0.084	0.084
3.000	0.445	1.557	0.444	1.561	0.301	0.302
5.000	0.440	1.576	0.443	1.566	0.633	0.629
6.000	0.449	1.544	0.454	1.528	1.034	1.024
8.000	0.473	1.465	0.480	1.445	1.407	1.387
10.000	0.500	1.388	0.506	1.369	1.332	1.314
20.000	0.614	1.128	0.612	1.133	0.415	0.416

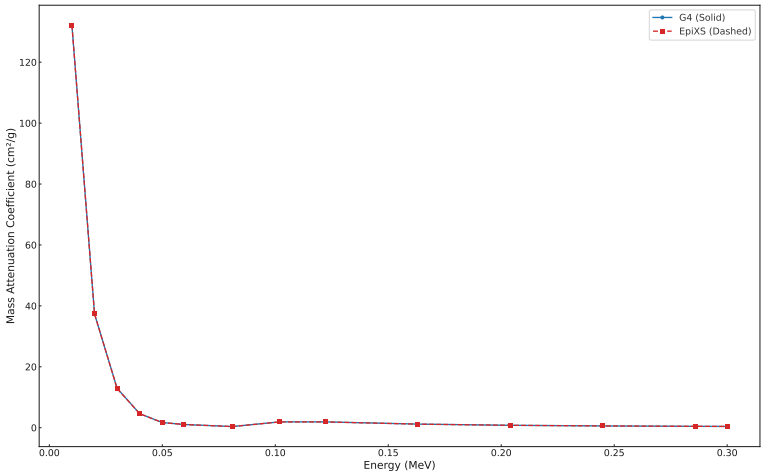

Figure 4.3: Comparison for Sample 3 between EpiXS data and simulated G4 data.

Table 4.4: Linear Attenuation Coefficients and HVLs of Sample 4 obtained from EpiXS and Simulated by G4.

Energy (MeV)	EpiXS		G4		Error %	
	LAC (cm^{-1})	HVL (cm)	LAC (cm^{-1})	HVL (cm)	LAC	HVL
0.010	430.557	0.002	429.867	0.002	0.160	0.161
0.020	68.048	0.010	68.020	0.010	0.041	0.041
0.030	22.878	0.030	23.010	0.030	0.575	0.571
0.040	55.425	0.013	55.434	0.013	0.016	0.016
0.050	31.373	0.022	31.378	0.022	0.015	0.015
0.060	19.990	0.035	20.018	0.035	0.136	0.136
0.081	8.971	0.077	8.954	0.077	0.193	0.194
0.112	4.865	0.142	3.906	0.177	19.707	24.544
0.122	3.208	0.216	3.184	0.218	0.750	0.756
0.136	2.466	0.281	2.474	0.280	0.321	0.320
0.161	1.719	0.403	1.707	0.406	0.712	0.718
0.223	0.915	0.758	0.913	0.759	0.199	0.200
0.276	0.660	1.051	0.658	1.054	0.254	0.255
0.302	0.585	1.185	0.585	1.186	0.072	0.072
0.356	0.485	1.429	0.484	1.432	0.173	0.174
0.384	0.449	1.543	0.449	1.545	0.132	0.132
0.511	0.351	1.976	0.352	1.968	0.412	0.411
0.662	0.292	2.371	0.295	2.353	0.753	0.747
0.835	0.253	2.742	0.256	2.713	1.065	1.054
0.840	0.253	2.742	0.255	2.723	0.708	0.703
1.170	0.207	3.344	0.209	3.322	0.646	0.642
1.275	0.198	3.499	0.199	3.482	0.487	0.484
1.333	0.193	3.585	0.061	11.402	0.645	0.641
2.000	0.159	4.353	0.160	4.335	0.430	0.428
3.000	0.137	5.053	0.137	5.056	0.057	0.057
5.000	0.122	5.665	0.122	5.672	0.116	0.116
6.000	0.120	5.775	0.120	5.777	0.022	0.022
8.000	0.119	5.816	0.119	5.814	0.029	0.029
10.000	0.121	5.742	0.121	5.748	0.089	0.089
20.000	0.134	5.163	0.133	5.212	0.942	0.951

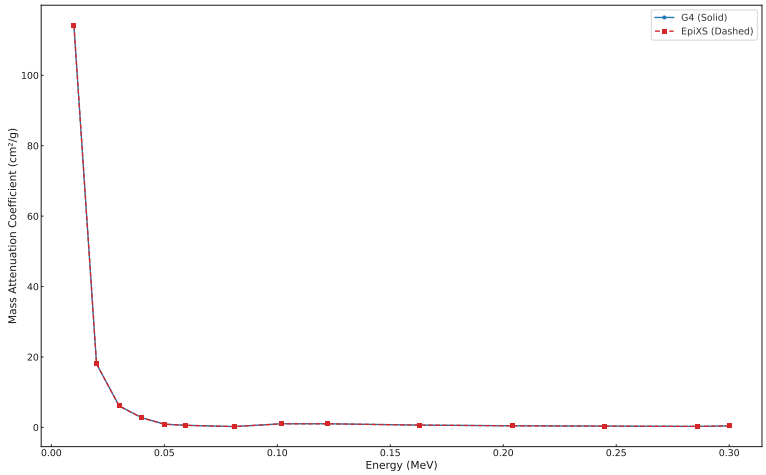

Figure 4.4: Comparison for Sample 4 between EpiXS data and simulated G4 data.

Table 4.5: Linear Attenuation Coefficients and HVLs of Sample 5 obtained from EpiXS and Simulated by G4.

Energy (MeV)	EpiXS		G4		Error %	
	LAC (cm^{-1})	HVL (cm)	LAC (cm^{-1})	HVL (cm)	LAC	HVL
0.010	854.124	0.001	853.813	0.001	0.036	0.036
0.020	241.401	0.003	241.282	0.003	0.049	0.049
0.030	83.161	0.008	83.592	0.008	0.519	0.516
0.040	94.286	0.007	94.116	0.007	0.180	0.181
0.050	52.522	0.013	52.781	0.013	0.493	0.491
0.060	33.148	0.021	33.346	0.021	0.598	0.594
0.081	18.685	0.037	18.662	0.037	0.125	0.125
0.112	15.414	0.045	12.410	0.056	19.489	24.206
0.122	10.075	0.069	10.037	0.069	0.372	0.374
0.136	7.655	0.091	7.686	0.090	0.413	0.411
0.161	5.183	0.134	5.136	0.135	0.908	0.916
0.223	2.506	0.277	2.500	0.277	0.215	0.216
0.276	1.662	0.417	1.659	0.418	0.180	0.181
0.302	1.419	0.488	1.422	0.488	0.168	0.167
0.356	1.102	0.629	1.100	0.630	0.178	0.178
0.384	0.991	0.699	0.989	0.701	0.197	0.197
0.511	0.703	0.986	0.705	0.983	0.280	0.279
0.662	0.549	1.262	0.553	1.253	0.720	0.715
0.835	0.456	1.521	0.461	1.505	1.084	1.072
0.840	0.456	1.521	0.459	1.511	0.640	0.636
1.170	0.360	1.927	0.363	1.912	0.811	0.805
1.275	0.342	2.027	0.344	2.015	0.625	0.621
1.333	0.333	2.081	0.336	2.066	0.764	0.758
2.000	0.275	2.518	0.277	2.506	0.472	0.470
3.000	0.245	2.833	0.245	2.834	0.005	0.005
5.000	0.232	2.988	0.232	2.981	0.207	0.207
6.000	0.233	2.973	0.234	2.961	0.408	0.406
8.000	0.240	2.885	0.242	2.869	0.543	0.540
10.000	0.250	2.773	0.251	2.762	0.411	0.409
20.000	0.296	2.339	0.294	2.358	0.804	0.810

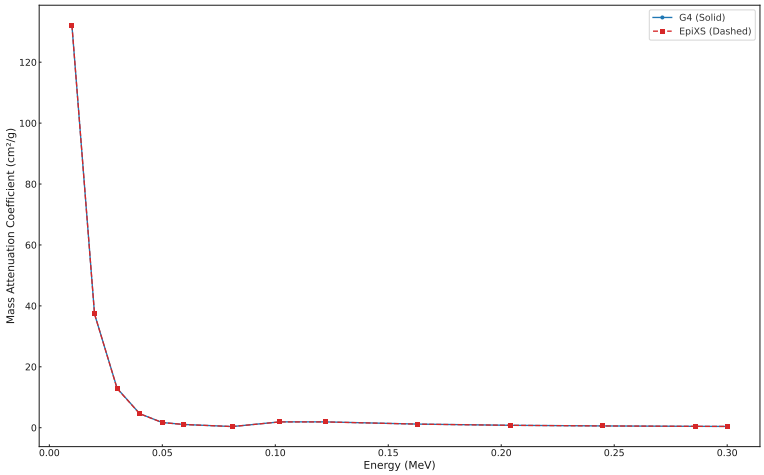

Figure 4.5: Comparison for Sample 5 between EpiXS data and simulated G4 data.

4.2 Results Summary

Comparison Based on EpiXS

Sample 1:
EpiXS data shows a steep decrease as energy increases, mirroring the trend observed in G4. This further confirms Sample 1's efficiency in low-energy shielding, but also highlights the challenge in maintaining performance at higher energies without significantly increasing thickness.

Sample 2:
EpiXS values decline slowly and maintain moderate levels of attenuation throughout the energy range. This makes Sample 2 more versatile and practical for real-world applications where radiation energy varies. It requires minimal adjustments for shielding.

Sample 3:
Although EpiXS starts with the highest values among all samples, it plummets rapidly, reinforcing the unsuitability of this sample for high-energy environments. Its outstanding low-energy performance is ideal for very specific use cases.

Sample 4:
EpiXS shows modest values throughout the spectrum with no extreme fluctuations. While not very strong, the predictable behavior allows engineers to plan for moderate performance without large corrections. Still, the sample would benefit from material improvement.

Sample 5:
EpiXS remains consistent and stable across all tested energies. Among the five, Sample 5 demonstrates the most balanced performance, requiring neither significant composition adjustment nor excessive thickness, making it ideal for mixed radiation scenarios.

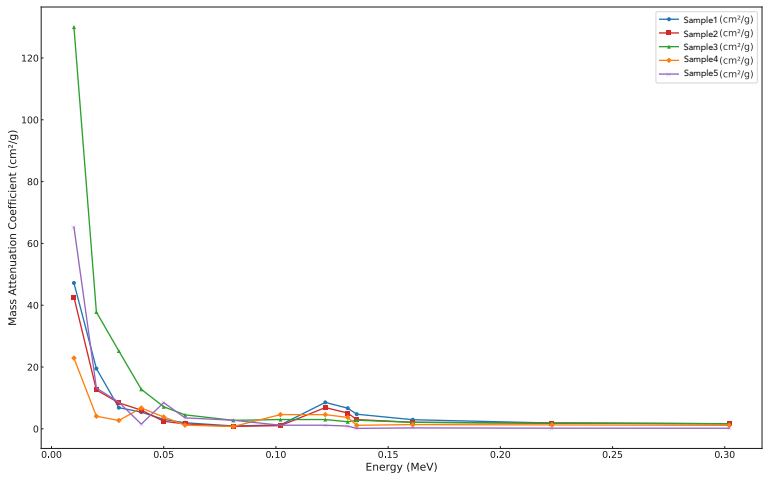

Figure 4.6: μ_m comparison for all five samples simulated using EpiXS, respectively.

Comparison Based on G4

Sample 1:
G4 starts very high (around 94) at low energies and drops drastically to approximately 0.02 at high energies. This makes Sample 1 highly effective for low-energy gamma radiation like medical X-rays, but it becomes significantly less effective at higher energies, requiring increased thickness for protection.

Sample 2:
G4 shows a more gradual decline across the energy spectrum, making it more stable than Sample 1. It provides consistent attenuation, offering better suitability for a broader energy range. The decrease in performance at higher energies is manageable with minor thickness adjustments.

Sample 3:
Sample 3 has the highest initial G4 value (around 157), indicating superior low-energy attenuation. However, it also has the steepest decline with increasing energy, which severely affects its effectiveness at medium and high energies. It demands redesigning the material's composition to sustain attenuation.

Sample 4:
G4 values are relatively low from the start and decrease gradually. Although not exceptional at any specific energy level, the consistent decline allows for predictable performance. However, its lower attenuation values limit its application unless its composition is reinforced with high atomic number elements.

Sample 5:
G4 is slightly better than Sample 4 and maintains excellent stability across low to medium energies. The attenuation remains relatively consistent, making it suitable for environments with a wide range of radiation energies such as nuclear facilities or therapeutic accelerators.

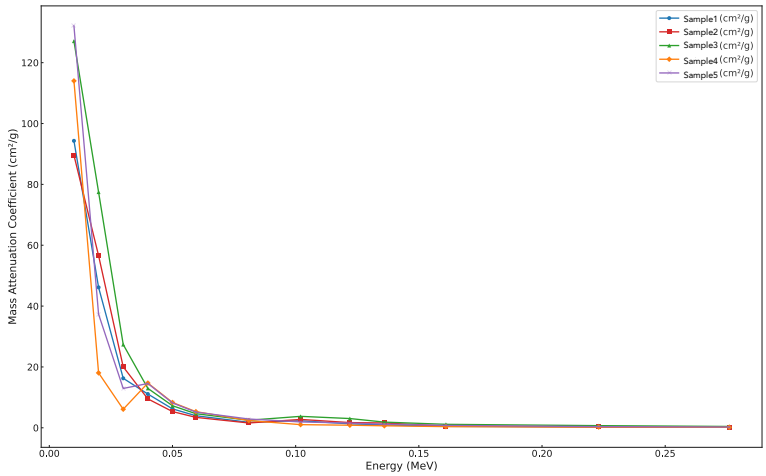

Figure 4.7: μ_m comparison for all five samples simulated using G4 respectively.

4.3 Neutron Results

Neutron shielding properties, including mass and linear attenuation coefficients, were determined using Geant4 simulation software. Results are shown in Tables 4.6 through 4.10. The μ_m values for all cement samples were plotted against energies from 0.01 to 20 MeV, shown in Figs. 4.8 through 4.12.

4.3.1 Results By Sample

4.3.1.1 Sample 1

The results for this sample are presented in Fig. 4.8 and Table 4.6.

4.3.1.2 Sample 2

The results for this sample are presented in Fig. 4.9 and Table 4.7.

4.3.1.3 Sample 3

The results for this sample are presented in Fig. 4.10 and Table 4.8.

4.3.1.4 Sample 4

The results for this sample are presented in Fig. 4.11 and Table 4.9.

4.3.1.5 Sample 5

The results for this sample are presented in Fig. 4.12 and Table 4.10.

4.3.1.6 Samples Comparisons

The results of comparisons using Geant4 simulations are shown in Fig. 4.13.

Table 4.6: Results for Sample 1 obtained from G4 simulation.

Energy (MeV)	G4			
	ΣR (cm^2/g)	LAC (cm^{-1})	HVL (cm)	MFP (cm)
0.010	0.075259	0.47337911	1.464253842	2.112471757
0.020	0.23517	1.4792193	0.468589871	0.676032283
0.030	0.074466	0.46839114	1.479846909	2.134967796
0.040	0.0746	0.469234	1.477188739	2.131132868
0.050	0.075564	0.47529756	1.458343654	2.103945158
0.060	0.072548	0.45632692	1.518970611	2.191411368
0.081	0.068303	0.42962587	1.613373935	2.327606575
0.112	0.066483	0.41817807	1.657540723	2.391325781
0.122	0.0697	0.438413	1.581037014	2.28095426
0.136	0.075001	0.47175629	1.469290808	2.119738562
0.161	0.066591	0.41885739	1.654852456	2.387447432
0.223	0.067255	0.42303395	1.63851431	2.363876469
0.276	0.0638	0.401302	1.727245766	2.491888902
0.302	0.064622	0.40647238	1.705274982	2.46019176
0.356	0.067481	0.42445549	1.633026776	2.355959632
0.384	0.078561	0.49414869	1.40270974	2.023682386
0.511	0.064627	0.40650383	1.70514305	2.460001422
0.662	0.05656	0.3557624	1.948342997	2.810864779
0.835	0.049774	0.31307846	2.213972755	3.194087514
0.840	0.050061	0.31488369	2.201280036	3.175775792
1.17	0.051945	0.32673405	2.121441523	3.060593164
1.275	0.060246	0.37894734	1.82913853	2.638889087
1.333	0.070866	0.44574714	1.555023282	2.243424377
2	0.038065	0.23942885	2.895002756	4.176606119
3	0.03529	0.2219741	3.122648906	4.505030091
5	0.030592	0.19242368	3.602192727	5.196865583
6	0.035083	0.22067207	3.141073451	4.531611092
8	0.026184	0.16469736	4.208611362	6.071742741
10	0.029688	0.18673752	3.711879544	5.35511021
20	0.033461	0.21046969	3.293334924	4.751277963

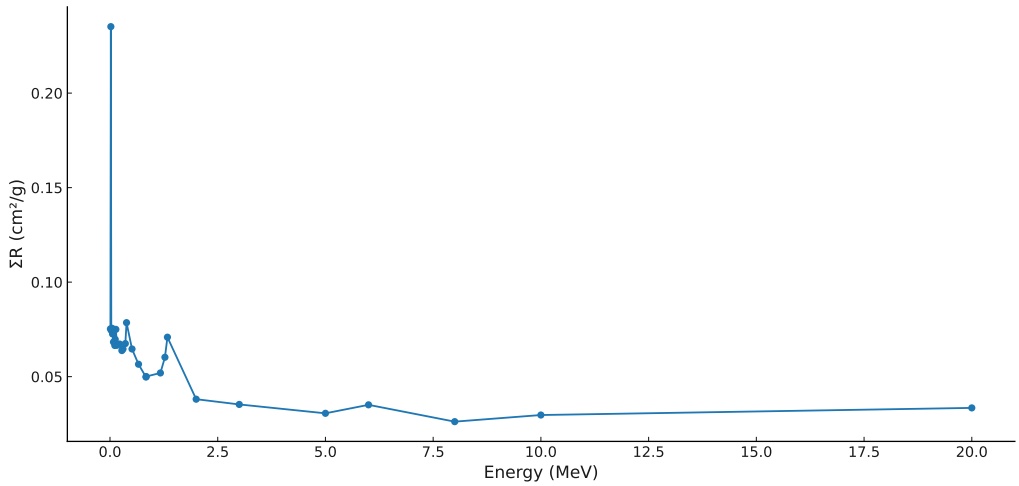

Figure 4.8: μ_m for Sample 1 simulated using G4.

Table 4.7: Results for Sample 2 obtained from G4 simulation.

Energy (MeV)	G4			
	ΣR (cm^2/g)	LAC (cm^{-1})	HVL (cm)	MFP (cm)
0.010	0.087946	0.4441273	1.560694829	2.25160669
0.020	0.35786	1.807193	0.383549062	0.55334433
0.030	0.083335	0.42084175	1.647049468	2.3761901
0.040	0.085076	0.4296338	1.613344156	2.327563613
0.050	0.080268	0.4053534	1.709982402	2.466983131
0.060	0.080423	0.40613615	1.706686737	2.462228492
0.081	0.073785	0.37261425	1.860227247	2.683740625
0.112	0.070901	0.35805005	1.935894662	2.792905629
0.122	0.074378	0.3756089	1.84539605	2.66234373
0.136	0.07996	0.403798	1.716569128	2.476485768
0.161	0.069693	0.35194965	1.969449836	2.841315512
0.223	0.069297	0.34994985	1.980704323	2.857552304
0.276	0.068141	0.34411205	2.014306621	2.906030172
0.302	0.064517	0.32581085	2.127452725	3.069265496
0.356	0.07125	0.3598125	1.926412175	2.779225291
0.384	0.080535	0.40670175	1.704313248	2.458804271
0.511	0.066004	0.3333202	2.079523475	3.000118205
0.662	0.051712	0.2611456	2.654255636	3.829281443
0.835	0.045974	0.2321687	2.985532419	4.307212816
0.840	0.046406	0.2343503	2.957739677	4.267116364
1.17	0.050054	0.2527727	2.742175799	3.956123426
1.275	0.061841	0.31229705	2.219512418	3.202079559
1.333	0.071885	0.36301925	1.909395109	2.754674855
2	0.037263	0.18817815	3.683462615	5.314113249
3	0.035789	0.18073445	3.835169114	5.532979462
5	0.031976	0.1614788	4.29249648	6.192763384
6	0.036624	0.1849512	3.747730107	5.40683164
8	0.026462	0.1336331	5.186942311	7.48317595
10	0.029569	0.14932345	4.6419178	6.696871791
20	0.033772	0.1705486	4.064220876	5.863431303

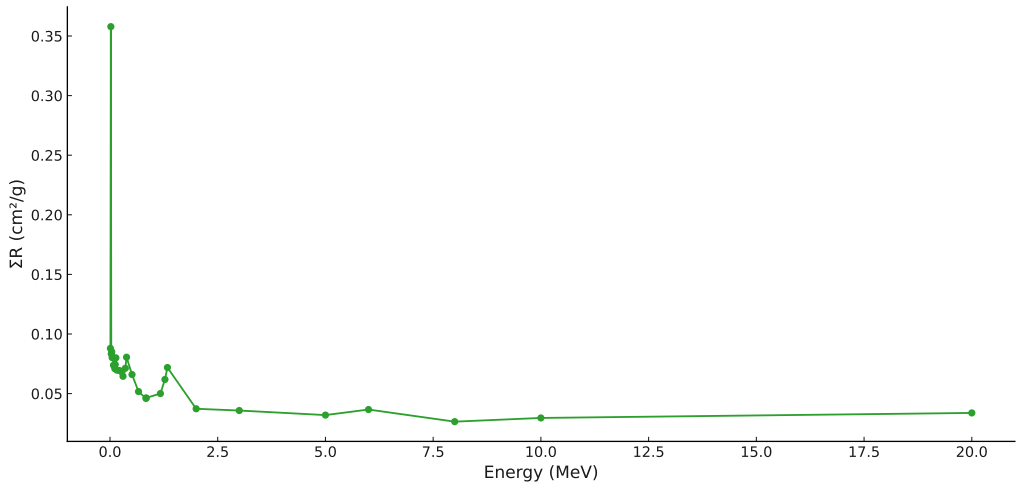

Figure 4.9: μ_m for Sample 2 simulated using G4.

Table 4.8: Results for Sample 3 obtained from G4 simulation.

Energy (MeV)	G4			
	$\sum R(\text{cm}^2/\text{g})$	LAC (cm^{-1})	HVL (cm)	MFP (cm)
0.010	0.039661	0.422944904	1.638859279	2.364374155
0.020	0.045021	0.480103944	1.443743983	2.082882285
0.030	0.041579	0.443398456	1.563260249	2.255307808
0.040	0.041615	0.44378236	1.561907915	2.253356803
0.050	0.043239	0.461100696	1.503244707	2.168723684
0.060	0.040207	0.428767448	1.616604021	2.332266604
0.081	0.036446	0.388660144	1.783427478	2.572941979
0.112	0.034027	0.362863928	1.910212416	2.75585398
0.122	0.038517	0.410745288	1.687535319	2.434598836
0.136	0.045882	0.489285648	1.416651364	2.043795897
0.161	0.035107	0.374381048	1.851448369	2.67107538
0.223	0.035885	0.38267764	1.811308287	2.613165483
0.276	0.033773	0.360155272	1.924578743	2.776580208
0.302	0.031166	0.332354224	2.085567538	3.008837944
0.356	0.03691	0.39360824	1.761007799	2.540597219
0.384	0.039692	0.423275488	1.637579308	2.362527546
0.511	0.030289	0.323001896	2.145953907	3.095957059
0.662	0.026889	0.286744296	2.417300676	3.487427698
0.835	0.024111	0.257119704	2.6958151	3.889239076
0.840	0.025083	0.267485112	2.591348638	3.738525829
1.17	0.024734	0.263763376	2.627912908	3.791276921
1.275	0.027095	0.28894108	2.398922232	3.460913208
1.333	0.031749	0.338571336	2.047270713	2.953587305
2	0.023289	0.248353896	2.790965601	4.026512232
3	0.025024	0.266855936	2.597458355	3.747340288
5	0.022895	0.24415228	2.838995321	4.095804471
6	0.023516	0.250774624	2.764024404	3.9876443
8	0.017672	0.188454208	3.678066879	5.306328846
10	0.018562	0.197945168	3.501713063	5.051904071
20	0.021633	0.230694312	3.004613224	4.334740598

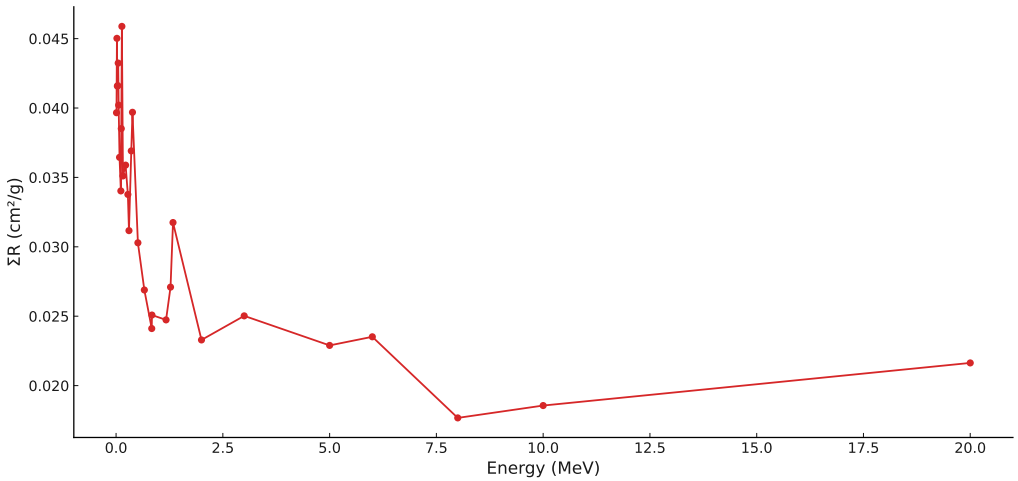

Figure 4.10: μ_m for Sample 3 simulated using G4.

Table 4.9: Results for Sample 4 obtained from G4 simulation.

Energy (MeV)	G4			
	ΣR (cm^2/g)	LAC (cm^{-1})	HVL (cm)	MFP (cm)
0.010	0.12979	0.489347237	1.416473065	0.705978832
0.020	0.44277	1.669375731	0.415213404	2.408400088
0.030	0.090742	0.342124563	2.026008233	0.49358141
0.040	0.08909	0.335896027	2.063576598	0.484595532
0.050	0.08745	0.329712735	2.102276033	0.475674928
0.060	0.086581	0.326436344	2.12337625	0.470948095
0.081	0.085076	0.320762043	2.160938914	0.462761808
0.112	0.083284	0.314005665	2.207435271	0.453014416
0.122	0.082834	0.31230903	2.219427277	0.450566689
0.136	0.082314	0.310348474	2.233448005	0.447738205
0.161	0.081384	0.306842095	2.258970302	0.442679569
0.223	0.079558	0.299957527	2.310817757	0.432747237
0.276	0.079083	0.298166635	2.324697332	0.430163526
0.302	0.079152	0.298426786	2.322670799	0.430538844
0.356	0.084651	0.319159665	2.171788155	0.460450066
0.384	0.098828	0.372611208	1.860242432	0.537564343
0.511	0.085386	0.321930836	2.153093471	0.46444802
0.662	0.067042	0.252768453	2.742221877	0.364667793
0.835	0.062071	0.234026291	2.961834658	0.33762857
0.840	0.062101	0.2341394	2.960403843	0.337791752
1.17	0.06805	0.256568915	2.701602338	0.370150701
1.275	0.083721	0.315653286	2.195913081	0.455391431
1.333	0.096046	0.362122234	1.914124889	0.522431951
2	0.047853	0.180420166	3.841849813	0.260291279
3	0.040275	0.151848833	4.564718537	0.219071558
5	0.03321	0.125211663	5.535803646	0.180642245
6	0.040291	0.151909157	4.562905837	0.219158588
8	0.030483	0.114930055	6.031034973	0.16580902
10	0.035998	0.135723259	5.107062589	0.195807273
20	0.039067	0.14729431	4.705865285	0.212500771

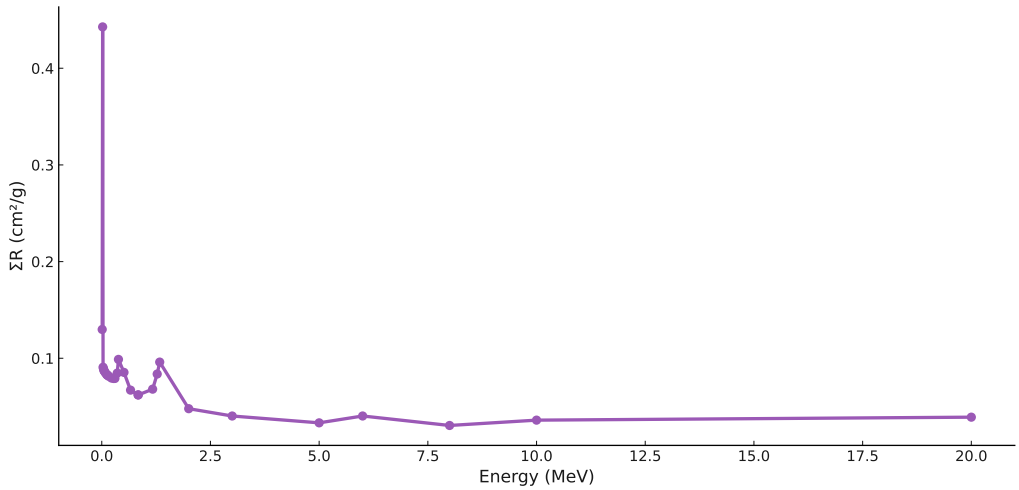

Figure 4.11: μ_m for Sample 4 simulated using G4.

Table 4.10: Results for Sample 5 obtained from G4 simulation.

Energy (MeV)	G4			
	ΣR (cm^2/g)	LAC (cm^{-1})	HVL (cm)	MFP (cm)
0.010	0.043562	0.28162833	2.461212551	3.550779142
0.020	0.056794	0.36717321	1.887793449	2.723510247
0.030	0.045007	0.290970255	2.382192573	3.436777412
0.040	0.053026	0.34281309	2.021939071	2.91704147
0.050	0.048179	0.311477235	2.225354224	3.210507503
0.060	0.046101	0.298042965	2.325661941	3.355220949
0.081	0.05423	0.35059695	1.977048518	2.852278093
0.112	0.071422	0.46174323	1.501152882	2.165705819
0.122	0.048968	0.31657812	2.189498063	3.158777998
0.136	0.052068	0.33661962	2.059140761	2.970712165
0.161	0.044822	0.28977423	2.392024924	3.450962496
0.223	0.044633	0.288552345	2.402154037	3.465575717
0.276	0.044231	0.285953415	2.423986371	3.497073116
0.302	0.044287	0.286315455	2.42092129	3.492651139
0.356	0.047537	0.307326705	2.255408233	3.253866272
0.384	0.054705	0.353667825	1.959881933	2.827511946
0.511	0.048036	0.31055274	2.231978956	3.220064972
0.662	0.040826	0.26394009	2.62615346	3.788738573
0.835	0.039108	0.25283322	2.741519412	3.95517646
0.840	0.039396	0.25469514	2.721477844	3.92626259
1.17	0.039799	0.257300535	2.693920479	3.886505716
1.275	0.043112	0.27871908	2.486902513	3.587841923
1.333	0.052167	0.337259655	2.055233024	2.965074491
2	0.031174	0.20153991	3.439255186	4.961796401
3	0.02766	0.1788219	3.876187316	5.592156218
5	0.023834	0.15408681	4.498419953	6.489848158
6	0.027173	0.175673445	3.945657129	5.692379972
8	0.021342	0.13797603	5.023678247	7.247635694
10	0.024555	0.158748075	4.366334398	6.299288984
20	0.026663	0.172376295	4.021128198	5.801261711

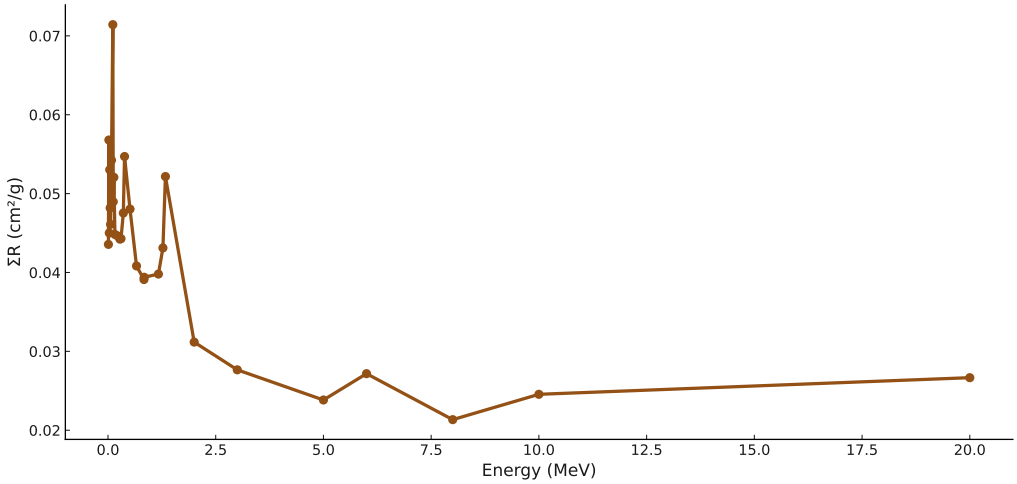

Figure 4.12: μ_m for Sample 5 simulated using G4.

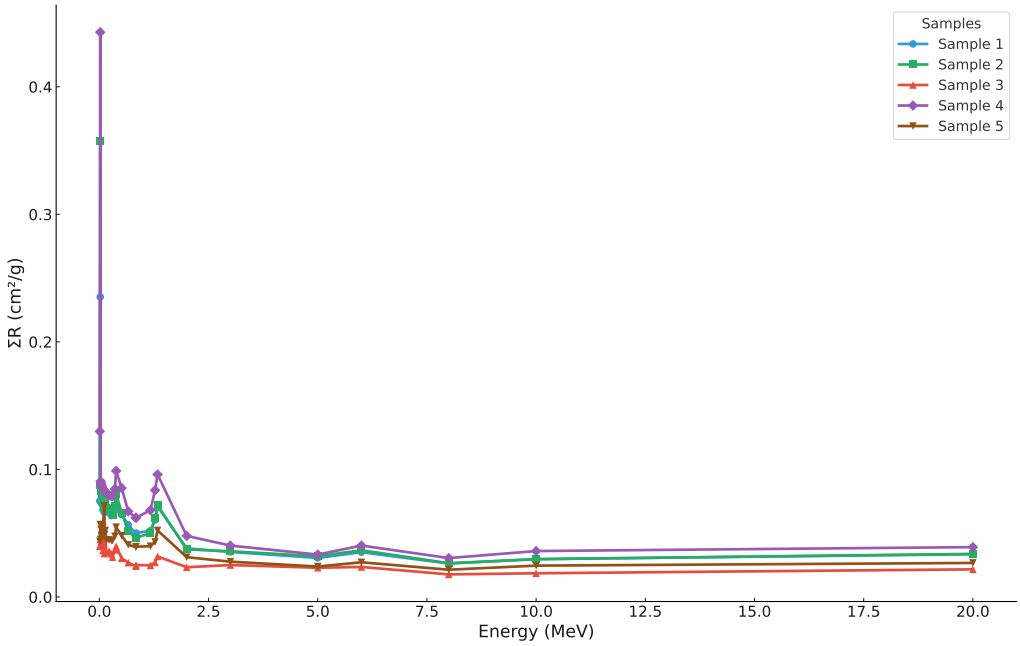

Figure 4.13: μ_m comparison for all five samples obtained by G4.

Table 4.11: Calculated values of $\sum R$, HVL fn, and λ fn for the studied glass samples.

PARAMETER	MRCsC	$\sum$R NXCOM(cm^{-1})	AVG.	HVL fn (cm)	λfn(cm)
Sample 1	0.15053	0.13639	0.14346	4.83164074	6.970584
Sample 2	0.12348	0.11213	0.117805	5.883851963	8.488604
Sample 3	0.17464	0.14411	0.159375	4.34915878	6.27451
Sample 4	0.10173	0.09968	0.100705	6.882947029	9.929994
Sample 5	0.11964	0.10477	0.112205	6.177507068	8.912259

Table 4.12: Values of ΣR, HVL_{fn}, and λ_{fn} for the studied glass samples from Eisawy et al. [7].

Parameter	ΣR (cm^{-1})	HVL_{fn} (cm)	λ_{fn} (cm)
Sample 1	0.138	5.012	7.231
Sample 2	0.173	3.999	5.769
Sample 3	0.291	2.385	3.44
Sample 4	0.100	6.954	10.032
Sample 5	0.113	6.147	8.868

4.4 Classification of Glass Samples by Neutron Shielding

Sample 1

This sample exhibits satisfactory attenuation of low to moderate energy photons, indicating its effectiveness in limited shielding scenarios. However, its performance diminishes significantly at higher photon energies, as evidenced by an increased half-value layer (HVL). This implies that greater material thickness is required to maintain shielding efficiency at elevated energies.
Classification: Moderate performer; appropriate for shielding against low to medium energy photons.

Sample 2

Demonstrating excellent stability across a wide photon energy spectrum, this sample outperformed others—particularly in high-energy attenuation. Its consistent shielding efficiency suggests a well-balanced composition optimized for broad-spectrum photon shielding applications.
Classification: High-performing and successful sample; suitable for a wide range of photon energies.

Sample 3

This sample showed high efficiency in attenuating low-energy photons but rapidly lost effectiveness as photon energy increased. This steep drop in shielding performance at higher energies indicates a need for compositional modification to improve its high-energy capabilities.
Classification: Strong performer at low energies; requires optimization for high-energy applications.

Sample 4

Among all samples, this one recorded the lowest attenuation coefficients, reflecting poor photon shielding capability. The data suggest that its current composition is inadequate and would require substantial reformulation to be viable for radiation protection.
Classification: Weak performer; significant compositional changes needed to achieve effective shielding.

Sample 5

This sample demonstrated consistent and balanced attenuation performance across the photon energy spectrum. While it performs well overall, minor adjustments could further enhance its shielding efficiency at higher energies, making it a promising candidate for practical applications.
Classification: Good performer; stable and reliable across energy levels.

Overall Summary

Among the evaluated samples, **Sample 2** and **Sample 5** emerged as the most effective overall, offering broad-spectrum shielding with high stability. **Sample 1** and **Sample 3** performed well in the low-energy range, but with limitations at higher energies. **Sample 4** was identified as the least effective, requiring major structural reformulation to improve its radiation shielding properties.

Chapter 5

Discussion

Comparison with Previous Study

To validate the findings of this study, the neutron shielding parameters obtained—summarized in Table 4.11—were compared with the results reported by Eisawy et al. [7], as shown in Table 4.12. Notably, our Sample 3 exhibited a ΣR value of 0.17464 cm^{-1} and a λ_{fn} of 6.27 cm, which closely resemble the shielding trend of Eisawy's Sy3 sample that recorded a ΣR of 0.291 cm^{-1} and a λ_{fn} of 3.44 cm. Although the attenuation in Sy3 was higher, our results follow a consistent pattern, particularly in identifying Sample 3 as the most efficient for neutron shielding.

In contrast, Sample 4 in our study demonstrated the lowest attenuation capability (ΣR = 0.09968 cm^{-1}), similar to Sy4 in Eisawy's study (ΣR = 0.100 cm^{-1}), both requiring greater thickness to achieve sufficient shielding. This alignment in performance order validates the simulation methodology and reinforces the reliability of the comparative results.

Despite the consistency in shielding trends, some discrepancies in the absolute values were observed. These differences can be attributed to several factors, including variations in glass compositions, elemental weight fractions, dopant concentrations, and simulation parameters. Moreover, an important technical limitation arises from the shielding software tools (NXCom and MRCsC) used in this study. These programs calculate shielding parameters over a broad energy range without allowing the user to specify a discrete neutron energy. As a result, it is not possible to compute energy-dependent macroscopic removal cross sections or isolate spectral effects, which introduces limitations in evaluating accuracy or quantifying error margins directly. Consequently, a key recommendation for future research is to enhance such shielding

software by incorporating functionality that enables energy-specific cross-section calculations. This advancement would allow researchers to conduct more precise comparisons with benchmark data and assess relative error more effectively. It would also improve the predictive value of simulations and optimize shield design with higher fidelity to realistic radiation spectra.

Additionally, Eisawy et al. emphasized the importance of balancing mechanical integrity, optical transparency, and radiation attenuation in glass systems. This aligns closely with the objectives of the present study, reaffirming that glass systems doped with high-Z elements such as Bi_2O_3, PbO, and WO_3 offer a promising pathway toward multifunctional radiation shielding materials that satisfy both performance and application demands.

Chapter 6

Summary

6.1 Conclusion

This study investigated the radiation shielding properties of five glass samples with varying compositions, using a combination of Geant4 Monte Carlo simulations and analytical calculations via EpiXS and NXCOM. The results demonstrated that specific dopants—such as Bi_2O_3, PbO, and WO_3—significantly enhance both gamma and neutron attenuation across a wide energy range.

Among the tested samples, Sample 2 and Sample 5 exhibited the most balanced performance across multiple energy levels, indicating their suitability for practical applications in nuclear, medical, and aerospace settings. Conversely, Sample 4 showed limited shielding effectiveness and requires substantial compositional enhancement.

Importantly, this study's findings align with recent literature trends advocating the development of high-Z, lead-free glass systems for radiation shielding [7]. This congruence with current research directions reinforces the validity of the selected simulation approach and the relevance of the investigated glass compositions.

In conclusion, the integration of high-Z oxides in glass matrices remains a promising pathway toward producing efficient, transparent, and safer alternatives to conventional shielding materials. The insights gained from this study pave the way for future research focused on experimental validation and application-specific design of advanced radiation-shielding glasses.

Recommendations

Based on the comparative performance of the five studied glass samples and in light of relevant literature, several recommendations can be proposed to enhance the effectiveness of glass-based radiation shielding materials.

The first recommendation focuses on optimizing the chemical composition of the glass. The

incorporation of high atomic number (high-Z) oxides—such as lead oxide (PbO), tungsten oxide (WO_3), and tantalum oxide (Ta_2O_5)—can significantly improve gamma radiation attenuation, particularly at higher energy levels [8, 9]. Additionally, rare-earth elements like gadolinium oxide (Gd_2O_3) and samarium oxide (Sm_2O_3) may enhance both gamma and neutron absorption. Increasing the content of tellurite-based glass matrix (TeO_2) may also improve the material's density and optical clarity [1]. These recommendations align with the findings of Eisawy et al. [7], who demonstrated in their Sy3 sample that doping with Bi_2O_3, Sb_2O_3, and Ta_2O_5 led to superior attenuation performance, evidenced by the highest ΣR and lowest HVL values in their dataset.

In addition, future studies are encouraged to explore the potential of alternative dopants such as antimony oxide (Sb_2O_3) and lanthanum oxide (La_2O_3), which have demonstrated promising radiation attenuation capabilities in recent research [7].

Another recommendation is the development of multilayered or "sandwich" shielding configurations. This structure consists of a glass layer doped with high-Z elements, a central liquid layer with a thickness between 1 and 1.5 cm, and an outer protective glass layer. The liquid core can be composed of borated water (H_2O with B_2O_3), which is highly effective for thermal neutron absorption [9]; glycerin-based solutions containing tungsten nanoparticles to enhance photon interactions; or mercury-based suspensions, which offer excellent attenuation capabilities but require strict safety controls due to toxicity [8]. This multilayered approach may yield substantial improvements in shielding performance across different radiation types and energies.

Furthermore, it is essential to validate the proposed material compositions and shielding configurations through both simulation and experimental methods. Monte Carlo simulation platforms such as GEANT4 and MCNP provide reliable environments to model photon and neutron interactions within complex material systems [3]. However, computational results must be supported by experimental measurements of key shielding parameters, including the Linear Attenuation Coefficient (LAC), Half-Value Layer (HVL), and Mean Free Path (MFP), to ensure the practical applicability of the materials [8, 9].

Once optimized and validated, these glass-based shielding materials have the potential to be implemented in several high-radiation environments. These include nuclear reactors, where comprehensive shielding from both gamma and neutron radiation is essential; medical radiology facilities, where safe exposure levels to multi-energy X-rays and gamma rays must be maintained; and spacecraft systems, where lightweight and effective protection from cosmic radiation is critical. The findings of this study, combined with evidence from recent literature, provide a strong foundation for future advancement in this field.

Bibliography

[1] M. I. Sayyed. "Assessment of gamma-radiation attenuation characteristics of Bi O –B O –SiO –Na O glasses using Geant4 simulation". In: *Applied Radiation and Isotopes* 180 (2022), p. 110028. DOI: 10.1016/j.apradiso.2021.110028.

[2] J. H. Hubbell and S. M. Seltzer. *Tables of X-ray mass attenuation coefficients and mass energy-absorption coefficients*. https://physics.nist.gov/PhysRefData/XrayMassCoef/. Accessed: 2024-05-24. 1996.

[3] S. Agostinelli et al. "Geant4—a simulation toolkit". In: *Nuclear Instruments and Methods in Physics Research Section A* 506.3 (2003), pp. 250–303. DOI: 10.1016/S0168-9002(03)01368-8.

[4] Farzad Isazadeh and Akbar Abdi Saray. "Comparative study on radiation shielding characteristics of CaF –CaO–B O –P O –SrO–Ta O glass systems using Geant4 and MCNPX". In: *Journal of Non-Crystalline Solids* 579 (2022), p. 121326. DOI: 10.1016/j.jnoncrysol.2021.121326.

[5] M. H. M. Zaid et al. "Radiation shielding effectiveness of BaO–B O glass system: Experimental and simulation approach". In: *Radiation Physics and Chemistry* 180 (2021), p. 109319. DOI: 10.1016/j.radphyschem.2020.109319.

[6] A. A. Hendi et al. "Shielding properties of TeO –V O –Bi O glass systems using Geant4 simulations". In: *Ceramics International* 46.16 (2020), pp. 25891–25898. DOI: 10.1016/j.ceramint.2020.06.030.

[7] A. Eisawy, M. Sadek, and A. M. Elsaid. "Investigation of Radiation Shielding Properties of Modified Glass Systems". In: *8th IUGRC International Undergraduate Research Conference*. Military Technical College, Cairo, Egypt, 2024, pp. 1–5.

[8] Glen Knoll. *Radiation Detection and Measurement (4th ed.)* John Wiley, 2010. ISBN: 978-0-470-13148-0.

[9] Nicholas Tsoulfanidis and Sheldon Landsberger. *Measurement and Detection of Radiation*. 5th. CRC Press, 2021. DOI: 10.1201/9781003009849.